Stress-dependent Peierls potential: Influence on kink-pair activation

David Rodney[1] and Laurent Proville[2]
[1]*SIMAP-GPM2, Grenoble INP, CNRS/UJF, 38402 Saint Martin d'Hères, France*
[2]*CEA, DEN, Service de Recherches de Métallurgie Physique, F-91191 Gif-sur-Yvette, France*
(Received 14 November 2008; published 17 March 2009)

Atomistic calculations based on the nudged elastic band method for a Lomer dislocation in aluminum evidence a dependence of the Peierls potential on the applied shear stress in such a way that the Peierls stress predicted from the zero-stress potential is half its true value for the case considered here. Stress-dependent Peierls potentials that are extracted are then introduced as substrate potentials in a string model with a line tension (LT) adjusted to match the dislocation kink width obtained from atomistic simulations. The LT model is found to predict accurately dislocation saddle configurations and corresponding kink-pair activation enthalpies for a wide range of stresses. In particular, it is shown that the stress dependence of the Peierls potential is required to model with accuracy the nonlinearity of the enthalpy-stress curve.

DOI: 10.1103/PhysRevB.79.094108 PACS number(s): 61.72.Bb, 62.20.F−

I. INTRODUCTION

It has long been recognized[1,2] that the potential energy of a dislocation, commonly called the Peierls potential, is a periodic function of the position of the dislocation in the crystal. Its derivative yields the lattice stress that materializes the resistance of the crystal to dislocation glide. The maximum lattice stress is the Peierls stress, i.e., the minimum stress to be applied to force a dislocation to glide athermally (i.e., at 0 K) in an otherwise perfect crystal from one stable position (Peierls valley) to the next. In high Peierls-stress crystals, such as body-centered cubic (bcc) (Ref. 3) and hexagonal metals,[4] at low temperature, when the applied stress is below the Peierls stress, dislocations move from one Peierls valley to the next by the thermally activated nucleation and propagation of kink pairs.[5] The dislocation velocity then depends exponentially on the kink-pair nucleation enthalpy H, a decreasing function of the applied stress σ_A. In this context, the Peierls stress can be equivalently defined as the applied stress at which the kink-pair formation enthalpy becomes zero, $H(\sigma_P)=0$.

The simplest model for dislocation glide that accounts for a Peierls stress is the so-called line tension (LT) model,[6–8] where the dislocation is viewed as an elastic string moving on a periodic substrate potential that corresponds to the Peierls potential, denoted V_P hereafter. Within this model, the equilibrium shape of the dislocation line $y(x)$ is the solution of a one-dimensional (1D) scalar field equation of the Klein-Gordon-type,

$$-V_P'[y(x)]+\sigma_A b+T\frac{\partial^2 y}{\partial x^2}=0, \tag{1}$$

where b is the Burgers vector and T is the line tension. Depending on the functional form of V_P, the model takes different names: $\phi^2-\phi^4$ or Eshelby theory for a fourth-order polynomial potential and continuous Sine-Gordon (SG) and discrete Frenkel-Kontorova (FK) theories for sinusoidal potentials.[9,10] The exact form of the kink-pair activation enthalpy $H(\sigma_A)$ depends on the shape of the substrate potential, which in classical LT models remains invariant with the applied stress. For the SG theory, asymptotic expressions have been obtained at low and high stresses[11,12] and the full curve is known numerically.[13] The enthalpy decreases from $H(0)=2E_k$, the kink-pair formation energy at zero applied stress, down to $H(\sigma_P)=0$ at the Peierls stress.

Recently,[14–16] the enthalpy $H(\sigma_A)$ has been determined from the three-dimensional (3D) molecular static (MS) simulations for different high Peierls-stress dislocations using the nudged elastic band (NEB) method,[17] a saddle-point search method. The kink-pair expansion energy was also obtained in Si using the same method.[18] In Ref. 15, it was found that $H(\sigma_A)$ decreases more rapidly than usually assumed and becomes negligibly small for stresses well below the Peierls stress. This property was tentatively related to the discrepancy reported in the literature between experimental and simulated Peierls stresses. In the present paper, we will not discuss this discrepancy but address the origin of the rapid decrease in the enthalpy $H(\sigma_A)$ through a combination of atomistic NEB calculations and a LT model.

As in Ref. 15, we consider a Lomer dislocation in a face-centered-cubic (fcc) aluminum crystal, which is well known for having a compact core and a high Peierls stress. Working with an edge dislocation in fcc metal allows several simplifications, as compared, for example, to screw dislocations in bcc crystals.[19–21] First, its motion is planer which allows to define without ambiguity a one-dimensional reaction coordinate between Peierls valleys. Second, it avoids uncertainties associated with the use of central force embedded atom method (EAM) potentials in bcc transition metals where d orbitals involve directional bonds.[22] Finally, the kinks that form in pairs on edge dislocations are symmetrical, and as will be seen in the following, they are more amendable to a representation within a LT model. The main finding here is that the Peierls potentials determined at the atomic scale from NEB calculations on straight dislocations evidence a marked stress dependence. The same conclusion was recently drawn by Gröger and Vitek[23] for screw dislocations in molybdenum and tungsten using a different approach. To estimate the importance of such a stress dependence, we employ a LT model in which the straight dislocation Peierls potential is introduced as a substrate potential. The stiffness is adjusted such that the LT kinks have the same extension as those in atomistic calculations. Following that method, the

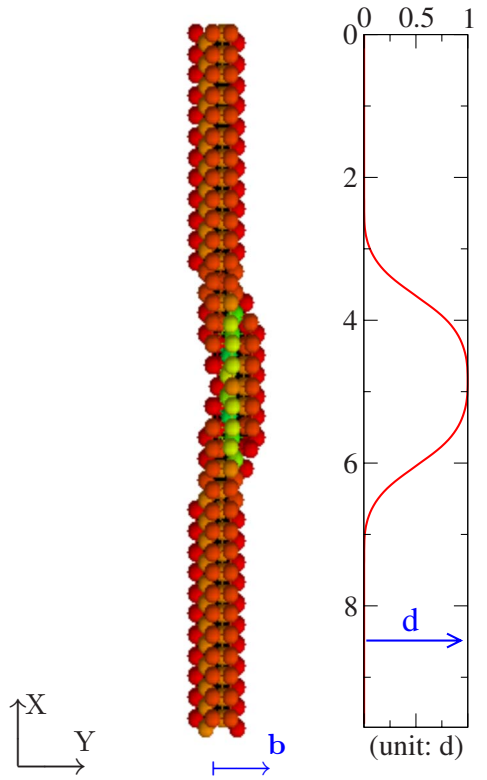

FIG. 1. (Color online) Dislocation configurations: on the left-hand side, transient state of the Lomer core with a kink pair between Peierls valleys; on the right-hand side, corresponding line shape obtained from an analysis of the displacement field within line tension model (see text for details).

LT model is found to predict accurately the kink-pair enthalpy curve and corresponding saddle configurations as determined by NEB calculations on kinked dislocations. In the LT model, switching off the stress dependence of the Peierls potential proves to dramatically modify the kink-pair activation enthalpy and to control its nonlinear dependence with applied stress.

II. COMPUTATIONAL TECHNIQUE

The EAM potential developed by Ercolessi and Adams[24] is used to model an aluminum crystal. The Lomer dislocation is an edge $\langle 110\rangle\{001\}$ dislocation. It is well known for having a high Peierls stress, 1600 MPa with the present interatomic potential.[15] As illustrated in Fig. 1, the simulation cell is oriented such that horizontal planes are $Z=[001]$ glide planes. The dislocation lies along the $X=[110]$ direction. Its Burgers vector and the glide direction are along the $Y=[\bar{1}10]$ direction. The cell height in the Z direction is $h=6.6$ nm and the glide distance in the Y direction is $L_G=14.4$ nm. We performed either two-dimensional (2D) simulations where L, the dislocation length in the X direction, was limited to a periodic unit cell or 3D simulations with $L=9.7$ nm. We simulated a periodic array of dislocations (PADs) by applying periodic boundary conditions in the X and Y directions.[25] Free boundary conditions are used in the Z direction, and external stresses are applied by adding shear forces to the atoms in the upper and lower surfaces of the simulation cell.

Although we are aware of its limitations, we also used the EAM potential developed by Mendelev *et al.*[26] to model iron crystals to serve as a comparison. It is the only EAM potential published to date that predicts a compact nondegenerate screw dislocation core, in agreement with *ab initio* calculations.[27] The computational cell geometry was adapted to the screw dislocation with a $\langle 111\rangle$ Burgers vector: horizontal $Z=[\bar{1}01]$ glide planes, dislocation line and Burgers vector along $X=[111]$, and glide direction along $Y=[\bar{1}2\bar{1}]$. The cell dimensions were the same as those for the Lomer dislocation.

The NEB method,[17] with improved tangent calculation[28] and climbing procedure,[29] is used to determine the minimum energy path (MEP) between Peierls valleys, i.e., between initial and final configurations where the dislocation is relaxed in successive Peierls valleys. The same methodology was used in Ref. 15. We employed 30 replica and a spring constant of 1 eV nm^{-1}. MEPs were determined for either straight dislocations or dislocations containing a kink pair. In the first case, the 2D simulation cell is used with an initial path linearly interpolated between initial and final configurations. In the second case, the 3D cell is used and the initial path contains an expanding kink pair by building replica where atomic positions correspond to the initial configuration except in a slab around the YZ central plane where atomic positions are taken from the final configuration. The initial path is then relaxed using a quenched dynamics algorithm.[17]

The substrate potential in LT models is a function of the position of the dislocation core in the glide plane, denoted by y. The latter, computed in the following way, will serve as reaction coordinate for the NEB calculations. We consider the two Z planes immediately above and below the dislocation core and compute the average difference in displacement per atom between these two planes in the Y direction of the Burgers vector, $\Delta u_Y=\langle u_Y^+-u_Y^-\rangle$. Displacements are computed with respect to the initial configuration. According to Orowan's law, Δu_Y increases linearly when the dislocation glides in the simulation cell with an increment of b when the dislocation crosses the entire cell. Thus, for a displacement of one Peierls valley (the distance between Peierls valleys is $d=b=0.285$ nm for the Lomer dislocation), Δu_Y increases by $bd/L_G=b/N_P$ where N_P is the number of Peierls valleys in the simulation cell. We define a reaction coordinate (called hereafter the *internal reaction coordinate*) that varies from 0 to 1 along the reaction pathway by setting

$$\theta_{\text{Int}}=\langle u_Y^+-u_Y^-\rangle\frac{N_P}{b}. \tag{2}$$

In 2D simulations with straight dislocations, $y=d\theta_{\text{Int}}$ is the position of the dislocation core in between the initial ($y=0$) and final ($y=d$) Peierls valleys. In 3D simulations with kinked dislocations, y is the average position of the core. As shown on the right-hand side (rhs) of Fig. 1, the shape of a kinked dislocation $y(x)$ can be determined by computing θ_{Int} in slabs of width b along the dislocation. Also, $r=L\theta_{\text{Int}}$ yields

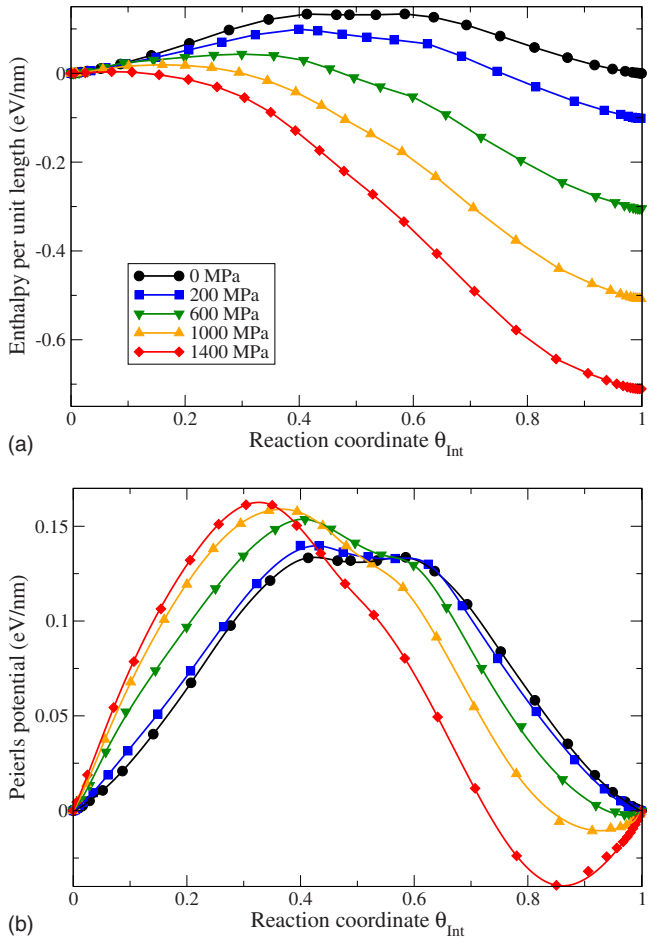

FIG. 2. (Color online) (a) Enthalpy per unit length and (b) Peierls potential for the Lomer dislocation in fcc aluminum modeled with EAM potential developed in Ref. 24 and for different applied stresses. The legend shown in (a) also applies in (b). Lines result from cubic splines.

directly the distance between kinks in the 3D cell. Note that we could *a priori* define the reaction coordinate by taking the difference in displacement between any two planes on each side of the glide plane and in particular between the upper and lower Z surfaces of the simulation cell. This choice of coordinate, denoted by θ_{Ext} hereafter, leads however to unphysical lattice stresses as discussed in Sec. V.

III. PEIERLS POTENTIAL

We first apply the NEB method to a straight dislocation in order to determine the Peierls potential V_P. NEB calculations give access to the difference of enthalpy between replica along the MEP and the initial configuration, ΔH_{tot},

$$\Delta H_{\mathrm{tot}} = V_{\mathrm{EAM}} - V^0_{\mathrm{EAM}} - \sigma_A b d \theta_{\mathrm{Ext}}. \tag{3}$$

Examples are given in Fig. 2(a) for different applied stresses σ_A. The first two terms on the rhs of Eq. (3) correspond to the internal energy of the replica computed from the position of the atoms and the EAM interatomic potential (V^0_{EAM} is the internal energy of the initial configuration). The third term on the rhs of Eq. (3) is the work of the applied stress—function of the difference of displacement between the upper and lower surfaces, i.e., θ_{Ext} (which is zero in the initial configuration at each stress). This term increases along the MEP and is responsible for the enthalpy difference between the initial and final configurations seen in Fig. 2(a) for nonzero applied stresses.

The internal energy V_{EAM} involves two terms: (i) the strain energy that stems from the relative displacement of the planes parallel to the glide plane induced by the applied stress and (ii) the potential energy of the dislocation core, which is the Peierls potential V_P. To extract this potential, we need to subtract from V_{EAM} the strain energy stored in the elastic medium between the external surfaces (where the stress is applied) and the internal surfaces that bound the glide plane. This formulates as $\sigma_A b d \theta_{\mathrm{Ext}} - \sigma_A b d \theta_{\mathrm{Int}}$ on the condition that the dislocation elastic stress field is not modified during the transfer between Peierls valleys, which is verified since the Burgers vector is conserved and the dislocation remains straight all along the MEP. The Peierls potential is thus expressed as

$$V_P(\theta_{\mathrm{Int}}) = V_{\mathrm{EAM}} - V^0_{\mathrm{EAM}} - \sigma_A b d \theta_{\mathrm{Ext}} + \sigma_A b d \theta_{\mathrm{Int}}$$

$$= \Delta H_{\mathrm{tot}}(\theta_{\mathrm{Int}}) + \sigma_A b d \theta_{\mathrm{Int}}. \tag{4}$$

When used in a LT model (see Sec. IV), V_P is expressed as a function of the dislocation position $y = d\theta_{\mathrm{Int}}$. Equation (4) then ensures that at any position between Peierls valleys, the enthalpy of the dislocation expressed in terms of its core position $V_P(y) - \sigma_A b y$ equals the total enthalpy in the cell ΔH_{tot}.

Peierls potentials are shown in Fig. 2(b) for different applied stresses. Note that the Peierls potential is periodic along the Y direction and since we reported a single period, only one minimum appears. Our choice of reaction coordinate is such that $\theta_{\mathrm{Int}} = 0$ for every initial configuration, which explains the shift of the Peierls potential with applied stress and the appearance of a minimum on the right-hand side of the figure. It appears clearly that the shape of the Peierls potential depends on the applied stress, in stark contrast with the conventional application of LT models. We note in Fig. 2(b) a metastable configuration midway between the initial and final configurations. The weak stability of this configuration is due to a configuration of high symmetry that disappears for nonzero applied stresses.

The Peierls potential for a screw dislocation in bcc iron was determined using the potential of Mendelev *et al.*[26] to ensure that the above stress dependence is not a particular case of the Lomer dislocation. The result, presented in Fig. 3, evidences again a pronounced stress dependence of the Peierls potential. Also, there is a marked local minimum along the paths, of much larger stability than in the Lomer case. This intermediate metastable configuration, already reported for the present EAM potential in Refs. 19 and 27, corresponds to the *split core* described by Suzuki[30] and Takeuchi.[31] The existence of such a core is a matter of debate[20] which is the main reason why we chose to study a simpler system, namely, the Lomer dislocation.

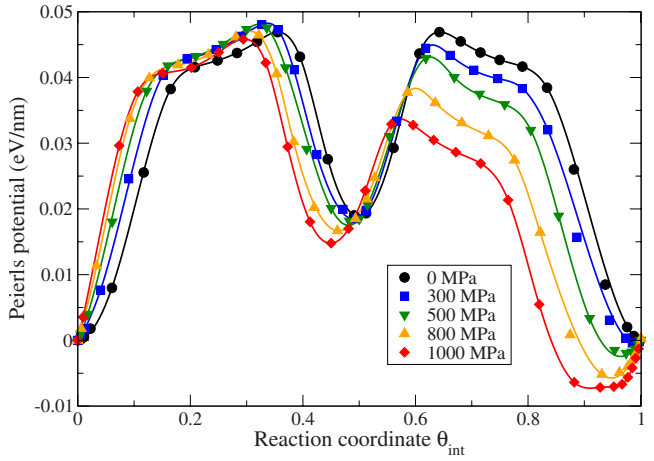

FIG. 3. (Color online) Peierls potential for a screw dislocation in bcc iron modeled with the EAM potential developed in Ref. 26.

The resistance to dislocation glide is materialized by the force experienced by the dislocation core along the MEP, i.e., the *lattice stress*,

$$\sigma(\theta_{\mathrm{Int}}) = \frac{V_P'(\theta_{\mathrm{Int}})}{b}. \tag{5}$$

In Fig. 4, the lattice stress $\sigma(\theta_{\mathrm{Int}})$ is plotted against the reaction coordinate θ_{Int} for different applied stresses and for the Lomer dislocation. Stresses were obtained after spline fitting and differentiation of the Peierls potentials shown in Figs. 2(b) and 3. Lattice stresses depend on the applied stress, similarly to Peierls potentials.

According to Eq. (1), mechanical equilibrium for a straight dislocation is such that its core position $y_S = d\theta_{\mathrm{Int}}$ satisfies $\sigma_A = \sigma(y_S)$. Here, $\theta_{\mathrm{Int}} = 0$ corresponds to the initial equilibrium at each applied stress, and we can check in Fig. 4 that the lattice stress at the origin of the reaction paths (as well as at their ends) is indeed equal to the applied stress to within a small error due to numerics. We also note in Fig. 4, by comparison of the different curves, that the maximum lattice stress along the MEP increases with applied stress,

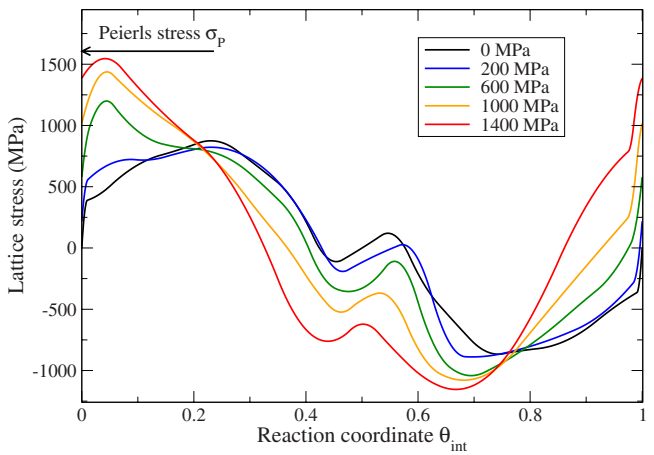

FIG. 4. (Color online) Lattice stress at different applied stresses for a Lomer dislocation.

and more importantly, the difference between initial and maximum stresses decreases. For instance, in Fig. 4 the difference is about 800 MPa at zero applied stress and drops down to about 100 MPa for an applied stress of 1400 MPa. The Peierls stress σ_P is reached when this difference vanishes, since beyond this point, Eq. (1) has no solution. From Fig. 4, we can infer that this occurs for an applied stress close to 1600 MPa, which is precisely the Peierls stress for the Lomer dislocation determined from MS simulations at increasing applied stress.[15] The fact that the Peierls stress can be accurately predicted by differentiating the Peierls potential with respect to $\theta_{\mathrm{I}}nt$ shows that a reaction coordinate, as defined in Eq. (2), is an accurate measure of the position of the dislocation core in its glide plane. We must notice that the foregoing computation for the Peierls stress cannot be carried out straightforwardly for screw dislocations in bcc crystals because the reaction coordinate for such dislocations is known to be two dimensional,[23] a consequence of their ill-defined glide plane. In the spirit of Ref. 23, a generalization of our approach would require a 2D mapping of the atomic displacements and a differentiation of the enthalpy with respect to 2D coordinates. Other subtleties about Peierls-stress computation at the atomic scale were identified by Ngan in Ref. 32.

We conclude that the concepts of Peierls potential and lattice stress at the heart of LT models are relevant for atomic-scale simulations; initial and final lattice stresses are equal to the applied stress and the Peierls stress for a straight dislocation is reached when the maximum lattice stress equals the applied stress. However, unlike conventional LT models, the Peierls potential is a function of the applied stress and stiffens with the latter. This stress dependence stems mainly from the dislocation core that adapts to the applied stress in order to increase its stability.

IV. STRESS-DEPENDENT LINE TENSION MODEL

A. Evaluation of the line tension

We use the Peierls potentials determined in Sec. III for the Lomer dislocation to solve the LT model of Eq. (1) and predict the kink-pair enthalpy and unstable dislocation configurations as a function of the applied stress. In Eq. (1), the only remaining parameter is the dislocation line tension T, which is expressed from the dislocation line energy (LE) E_L as[33]

$$T = E_L + \frac{d^2E_L}{d\phi^2}. \tag{6}$$

The second term reflects the dependence of the dislocation energy on its character, i.e., on the angle ϕ between the line direction and Burgers vector. The line energy itself is composed of an elastic (E_{el}) and a core (E_{core}) contribution. In an isotropic elastic medium, for an edge dislocation,[34]

$$E_L = E_{\mathrm{el}} + E_{\mathrm{core}} = \frac{\mu b^2}{4\pi(1-\nu)}\ln\left(\frac{R}{r_c}\right) + E_{\mathrm{core}}, \tag{7}$$

where $\mu = 3.48 \times 10^4$ MPa is the $\langle 110\rangle\{001\}$ shear modulus and ν is the Poisson ratio, which we computed for the present interatomic potential $\nu = 0.3137$. The lengths R and r_c are the outer and inner cutoff radii.

In Eq. (6), the line energy E_L is easily computed from MS simulations but the second term is more difficult to extract because the line direction cannot be changed continuously in atomistic simulations. On the other hand, the elastic contribution to T can be computed by using the elasticity theory. For an edge dislocation in an isotropic medium, $E_{\rm el}+d^2E_{\rm el}/d\phi^2=(1-2\nu)E_{\rm el}$.[34] $E_{\rm el}$ is determined by computing the line energy E_L in cells of different dimensions and using Eq. (7) in order to separate the elastic and core contributions, as was done in bcc tantalum by Yang *et al.*[35] We used cells of different sizes but the same aspect ratio h/L_G and same boundary conditions as presented in Sec. II. E_L was computed as the energy difference between the simulation cell containing a dislocation and the cell containing the same number of atoms but without the dislocation. Since the cell with dislocation contains an extra-half plane, the energy for the cell without dislocation was taken as the mean energy between a cell without the extra-half plane and one with a full additional plane. In Eq. (7), R was taken as the smallest dimension of the simulation cell, i.e., $R=h/2$, and $r_c=b$. We obtained $E_L=2.144\ln(h/2b)+2.25$ eV nm^{-1}. The prelogarithmic factor agrees well with that in Eq. (7), $\mu b^2/4\pi(1-\nu)=2.04$ eV nm^{-1}, as reported for other metals.[35] For the cell size used in the 3D-MS simulations, $h=12b$ and thus $E_L=7.5$ eV nm^{-1}, $E_{\rm el}=5.25$ eV nm^{-1}, $E_{\rm core}=2.25$ eV nm^{-1}, and $T_{\rm el}=1.95$ eV nm^{-1}. The only term that remains to complete the evaluation of T is $d^2E_{\rm core}/d\phi^2$, for which unfortunately there is no computational method. Two limiting cases can however be considered where $d^2E_{\rm core}/d\phi^2$ is either zero or scales as the elastic term. In the first case, we obtain $T=(1-2\nu)E_{\rm el}+E_{\rm core}=4.2$ eV nm^{-1} and in the second case, $T=(1-2\nu)E_L=2.8$ eV nm^{-1}.

Since the uncertainty on the value of the line tension T is large, we preferred to fit this parameter on a dislocation property, the equilibrium kink width at zero applied stress. To that purpose, we worked with a LT model using the Peierls potential at zero applied stress obtained in Sec. III. We studied an elastic string of the same length as the dislocation in atomistic simulations ($L=9.7$ nm), containing a fully formed kink pair. The string kink shape was compared with that obtained through NEB atomistic calculation. As explained in Sec. II, the shape of the atomistic dislocation was determined by computing the internal reaction coordinate in slabs of width b along the dislocation line.

Figure 5 compares the LT and 3D-MS kink shapes. The value of the line tension yielding the best agreement is $T=3.6$ eV nm^{-1}, which is in between the two bounds computed above. A comparison of the kink shape shown in Fig. 5 with the well-known solution of the SG theory,

$$y(x)=\frac{2d}{\pi}\left[\tan^{-1}\exp\left(\frac{x}{\xi}\right)\right], \tag{8}$$

gives an adjusted value $\xi=0.29$ nm. The kink width (that corresponds to the linear extrapolation of the kink from $y=0$ to $y=1$) is $\pi\xi\sim 3.2b$. It corresponds to a rather narrow kink, particularly in comparison with the $20b$ found for screw dislocations in bcc iron.[36] This result is however consistent with the fact that the line tension of a screw dislocation is significantly larger than that of an edge. It is also worth noticing that for edge dislocations, left and right kinks are perfectly symmetrical since they are of the same nature, in contrast to the screw case.

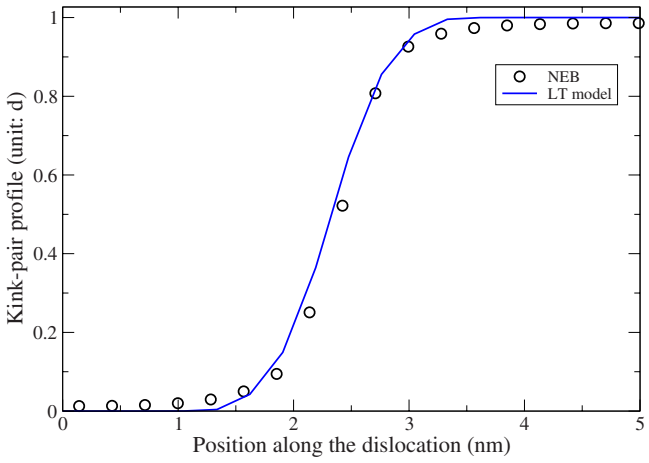

FIG. 5. (Color online) Kink shape predicted by 3D-MS calculations for Lomer dislocation (open symbols) and by a LT model with $T=3.6$ eV nm^{-1} (full line) at zero applied stresses.

B. Prediction of the LT model

The accuracy of the LT model can now be tested on activated kink-pair states at nonzero applied stresses. The Peierls potentials obtained at different applied stresses in Sec. III were employed as variable substrate potentials. The kink-pair saddle configuration was determined to computer precision by using the NEB replica with the maximum enthalpy as starting configuration in a Newton-Raphson solver.[37] Unfortunately the computational load involved in such a technique is prohibitive for 3D-MS calculations. In the latter case, the kink-pair activated state was identified with the NEB replica having maximum enthalpy. Using 30 replica and the climbing NEB procedure reduces the computational error. Profiles issued from 3D-MS simulations down to 100 MPa are reported in Fig. 6 as open symbols along with the LT profiles shown as full line. A remarkably good agreement is obtained at all stresses. Noticeably, the kinks in 3D-MS simulations are not fully formed in the activated state. Determination of activated states below 100 MPa, where kinks are fully formed, was difficult because the enthalpy curve along the MEP near the maximum is very flat. This point will be further discussed in Sec. V.

The corresponding activation enthalpy $H(\sigma_A)$ is shown in Fig. 7 as open circles for the atomistic computations and as filled triangles for the LT model with stress-dependent substrate. Both results are close to each other over the entire stress range. The agreement is particularly satisfactory since the only fitted parameter, T, was adjusted on an indirect property of the dislocation, i.e., its kink width at zero applied stress. We note that the kink-pair formation energy, which is the activation enthalpy at zero applied stress, $2E_k=0.42$ eV, is very well reproduced by the LT model even if this value was not fitted. For comparison, we added in Fig. 7 the prediction of the SG theory with fixed sinusoidal potential. In this case, the activation enthalpy is well approached by

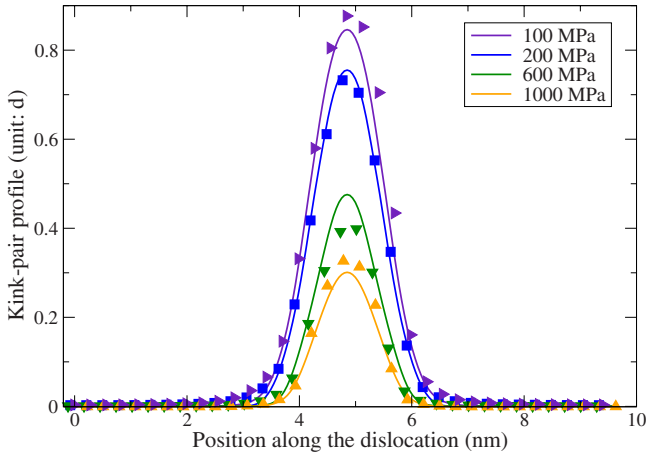

FIG. 6. (Color online) Lomer dislocation unstable configurations predicted by 3D-MS NEB calculations (symbols) and a LT model with stress-dependent Peierls potential (curves) for different applied stresses noted in the figure.

Kocks' law $H(\sigma)=2E_k[1-(\sigma/\sigma_P)^p]^q$, with $p=0.8$ and $q=1.286$.[38] The two parameters (E_k and σ_P) were fitted on the simulation values. As reported previously in Ref. 15, the kink-pair activation enthalpy computed through 3D-MS simulations has a curvature much more pronounced than the SG prediction. According to the much better agreement obtained between 3D-MS calculations (circles in Fig. 7) and stress-dependent substrate LT model (triangles in Fig. 7), we conclude that the marked nonlinear behavior of the kink-pair nucleation enthalpy is due to the stiffening of the Peierls potential.

V. DISCUSSION

A. Stress-dependent Peierls potential

In the present work, 2D NEB calculations were used to determine the Peierls potential of a fcc Lomer and a bcc screw dislocation. It was shown that the potential depends on the applied shear stress. This effect stems from an influence of the applied stress tensor on the dislocation core structure. We believe that it is a general effect that concerns any dislocation and may include nonglide stresses, i.e., components of the applied stress tensor perpendicular to the dislocation Burgers vector, in cases when the dislocation core is sensitive to such stresses. This is particularly the case for screw dislocations in bcc metals, as recently shown by Gröger and Vitek[23] in bcc tungsten and molybdenum. These authors did not use the NEB method to obtain the Peierls potentials directly from atomistic simulations. Instead a generic functional form was adjusted to reproduce the Peierls-stress dependence on nonglide stresses computed at the atomic scale. Such method allowed one to account for the two-dimensional energy landscape of the screw dislocation core in the {111} plane perpendicular to its Burgers vector. Remarkably, the potentials obtained were shown to depend on all the terms of the applied stress tensor. To consolidate our belief on the widespread of our conclusions, we performed the same type of computations on the phenomenological 1D FK model and found that the enthalpy of the single kink profile in between two stable positions also depends on the applied shear stress.

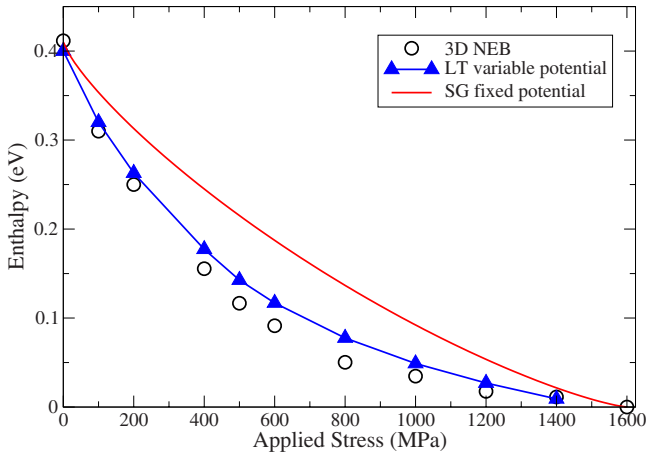

FIG. 7. (Color online) Kink-pair formation enthalpy curves obtained from 3D-MS NEB calculations for Lomer dislocation (circles) from a LT model with stress-dependent Peierls potential (filled triangles) and from SG theory (solid line).

The Peierls potentials obtained in the 2D NEB atomistic calculations stiffens with the applied stress, reflecting a stabilization of the dislocation core. If the Peierls potential of the Lomer dislocation at zero applied stress is used to predict the Peierls stress (which corresponds to the maximum lattice stress along the MEP), a value of 800 MPa is obtained, whereas the *true* Peierls stress is 1600 MPa. The stress dependence cannot therefore be neglected for the Lomer dislocation studied here. According to Fig. 3, a similar feature can be expected for the screw dislocation in a bcc iron computed with the interatomic potential of Mendelev *et al.*[26]

Inserting the stress-dependent Peierls potential in a LT model yields an accurate estimate of (1) the kink-pair formation energy, (2) the enthalpy-stress curve, and (3) the unstable dislocation shapes for all stresses above 100 MPa. The stress dependence in Fig. 7 implies a more rapid decrease in the kink-pair formation enthalpy than in the case of the SG theory. This effect can be illustrated through a phenomenological approach. For instance we may choose a standard form for the Peierls potential as the cosine potential of the SG theory $V_P(y)=A[1-\cos(2\pi y/d)]$ and assume that A is a linear function of the applied stress $A=A_0(1+\alpha\sigma_A)$ where α is a positive constant accounting for the stiffening of the dislocation potential. In Fig. 8, we show the kink-pair nucleation enthalpy for the classical SG theory (full line) and the modified SG model with $\alpha=0.6$ and 0.8 MPa^{-1}. The enthalpy is scaled by the kink-pair formation energy and the stress by the Peierls stress. The modified SG enthalpy varies more steeply at low stresses than with a fixed potential and becomes more flat with lower values at larger stresses. The same observations hold for the atomistic data reported in Fig. 7.

The Peierls potential has to be differentiated with respect to the reaction coordinate in order to compute the lattice stress used in the LT model. The choice of the reaction coordinate is thus of prime importance. Here we could use a

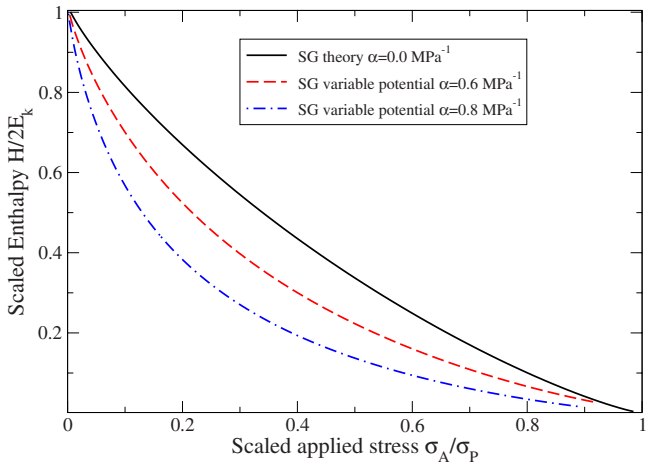

FIG. 8. (Color online) Kink-pair formation enthalpy against applied stress for the SG theory (solid line) and for the modified SG model with stress stiffening Peierls potential. The potential parameter is α=0.6 MPa^{-1} (dashed line) and α=0.8 MPa^{-1} (dotted-dashed line).

scalar variable θ_{Int} that defines the position of the dislocation core in its glide plane because of the choice of an edge dislocation, but a 2D reaction coordinate would be better suited for screw dislocations that do not have a definite glide plane.[23] Note also that in the present case, θ_{Ext} which is computed from the difference of displacement between the upper and lower surfaces of the cell cannot be used because it varies very nonlinearly between the two Peierls valleys. As shown in Fig. 9, θ_{Ext} increases rapidly at the start and end of the path and is almost flat in between. Differentiation of the Peierls potential with respect to θ_{Ext} thus leads to unphysical lattice stresses. Also, the important difference between θ_{Int} and θ_{Ext} implies through Eq. (4) that the Peierls potential V_P is different from, and should not be confused with, V_{EAM} which is the potential energy of the atoms in the simulation cell.

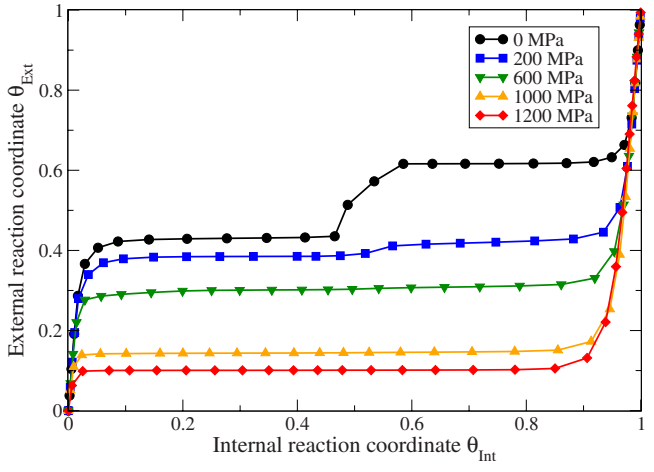

FIG. 9. (Color online) External reaction coordinate θ_{Ext} as a function of internal reaction coordinate θ_{Int} along the MEP of a straight Lomer dislocation at different applied stresses.

B. Line tension and line energy models

The main issue addressed in the present work was to demonstrate the feasibility for a multiscale approach through which a LT model, often used phenomenologically at the mesoscopic scale to treat experimental data on thermally activated dislocation glide,[39] provides a satisfactory description of the kink shape and kink energetics down to the atomic scale where it is usually believed to fail.

We used a LT model with T adjusted on an indirect quantity, the atomistic kink width. The value obtained is in the range predicted by elasticity theory (see Sec. IV). In the literature, another model has been proposed, which is the LE model of Dorn and co-workers.[40,41] LE and LT models are not equivalent because the LE model does not account for the dependence of the line energy on the dislocation orientation. However a general framework can be proposed in which both models (i.e., LT and LE) are derived as approximations. The energy of a dislocation of shape $y(x)$ is expressed as

$$E = \int \{[V_P(y) + E_L(y')]\sqrt{1 + y'^2} - \sigma_A b y\} dx, \qquad (9)$$

where the only assumption is that the dependence of the line energy on the dislocation orientation [parametrized here by $y'(x)=dy/dx$] is independent of the dislocation core position y. For a straight dislocation at position y_0, the line energy reads $V_P(y_0)+E_L(0)$, i.e., in agreement with the notations used above, $E_L(0)$ is the dislocation energy at equilibrium, and V_P measures the energy variation between Peierls valleys. In the LE model, $E_L(y')=E_L(0)$ is constant. If the orientation dependence is accounted for but y' is assumed small, Eq. (9) can be expanded to second order and the corresponding Euler-Lagrange equation is at first order,

$$-V_P'(y) + \sigma_A b + [V_P(y) + E_L(0) + E_L''(0)]\frac{\partial^2 y}{\partial^2 x} = 0. \qquad (10)$$

This equation is equivalent to Eq. (1) using the definition of T in Eq. (6), except that the line tension term now includes the Peierls potential. We found that T=3.6 eV nm^{-1} while V_P in Fig. 2 is at most equal to 0.16 eV nm^{-1} and can therefore be safely neglected. In contrast, neglecting $E_L''(0)$ as done in the LE model would lead to a strong overestimation of the dislocation line stiffness as shown in Sec. IV. As a consequence, the LT model is better adapted than the LE model.

A final point about the LT model is that an edge dislocation is the best adapted configuration because the left and right kinks on edge dislocations are equivalent (in energy and width), an inevitable property of kinks in the LT models of Eqs. (1) and (9). Indeed, the second-order expansion applied to the dislocation energy does not differentiate between a positive or negative y' dependence of the dislocation energy. Treating screw dislocations, where the kinks are not equivalent, would require a higher-order expansion of Eq. (9).

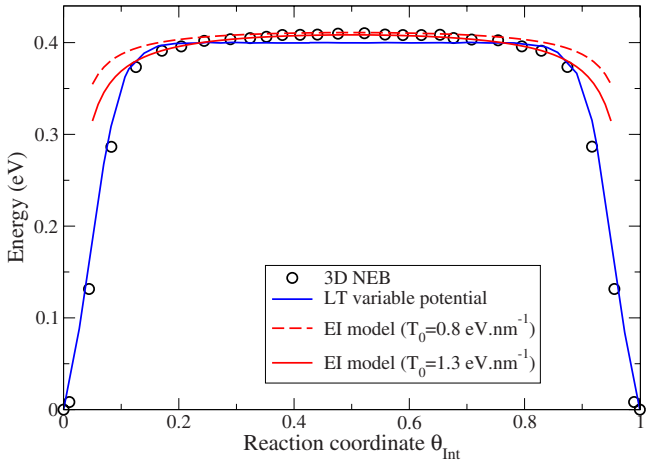

FIG. 10. (Color online) Energy of the kink pair computed along the reaction path at zero applied stress. The open symbols correspond to the atomistic computation.

C. Line tension and elastic interaction models

In Sec. IV, the LT model was shown to reproduce the enthalpy and unstable shapes at least down to 100 MPa. Below this applied stress, MEPs obtained with the NEB method are very flat near their maximum, making it difficult to determine with precision unstable configurations.

In the classical theory of kink-pair nucleation,[42] an approach different from the LT model is used to describe activated states at low applied stresses, the elastic interaction (EI) approximation.[39,43,44] Indeed, kinks in a LT model interact at short range only with an exponentially decaying energy[45] while in a 3D elastic medium, the kink-kink interaction is long ranged and Coulomb-type.[46,47] As a result, in a LT model at finite stress, the kinks are never fully formed in the activated state while in a 3D medium at low stresses, the activated state is made of two fully formed kinks with an unstable equilibrium distance that diverges at zero applied stress. The unstable configurations shown in Fig. 6 down to 100 MPa contain only a bulge and are consistent with a LT model. If the EI approximation has a range of validity, it is below 100 MPa. Unfortunately, as mentioned above, we could not determine with precision the unstable configurations in this stress range.

On the other hand, the regime of long-range interaction between kinks can be seen in the variation in the kink-pair energy along MEPs. Figure 10 shows the 3D NEB pathways obtained at zero applied stress as open circles, as a function of θ_{Int} which in 3D yields the distance between kinks. We can identify the two regions of nucleation ($\theta_{\mathrm{Int}}<0.15$) and annihilation ($\theta_{\mathrm{Int}}>0.85$) where the energy varies rapidly, separated by the region of kink-pair expansion where the energy varies more slowly. The maximum energy corresponds to $\theta_{\mathrm{Int}}=0.5$, i.e., when the kink and antikink are at equal distance with their periodic images. The reason is that when no external stress is applied, the EI approximation for an infinite dislocation has no unstable position. Here the critical configuration is set only by the symmetry of the interaction with the periodic images. In Fig. 10, we have added the MEP obtained with the LT model and two predictions of the EI model depending on the parametrization of the model, to be discussed below. As expected, the LT model reproduces accurately the phases of nucleation and annihilation while the EI model accounts for the variation in the energy during the phase of expansion. The LT model predicts a constant energy in the expansion phase because of its short-range kink-kink interaction, while the EI approximation fails to reproduces the nucleation and annihilation phases because it assumes fully formed kinks.

In the EI model, the energy of an expanding kink pair is

$$V(r) = 2E_K - \frac{T_0 d^2}{2r}, \tag{11}$$

where the second term is the long-range interaction potential given by the elasticity theory.[46,47] Another expression has been proposed[48,49] to account for the finite width of the kinks but leads to similar results as below. The curves shown in Fig. 10 were obtained by accounting for the kink interaction with their periodic images. In Eq. (11), T_0 is the prelogarithmic factor of the elastic line tension as described in Eq. (7) multiplied by $(1-2\nu)$ to account for the orientation dependence of the edge dislocation line energy. The value thus obtained is 0.8 eV nm^{-1}, leading to the dashed curve, which varies too slowly in comparison with NEB results. Upon adjustment, we find $T_0=1.3$ eV nm^{-1}. A larger fitted value for T_0 indicates a kink-kink interaction stronger in atomistic simulations than in an elastic medium, an observation already made by Duesbery and Basinski[50] that would be worth investigating in more details.

VI. CONCLUSIONS

The main conclusions of our atomistic study are the following. The Peierls potential depends on the applied stress and this dependence controls the steep decrease in the kink-pair formation enthalpy at low stresses. Such an effect was found particularly pronounced for a Lomer dislocation in Al and is expected to occur with more or less amplitude for other dislocations with high Peierls barrier in different materials.

According to the present work, the Peierls potential obtained at zero applied stress could not be used to predict the Peierls stress but rather, either stress- or strain-controlled simulations are required. The LT model can be used to describe phenomenologically high Peierls-stress dislocations at least down to 100 MPa. Below this value, we may enter the low-stress regime of the EI model with possibly a stronger long-range interaction than predicted from elasticity theory. We expect that the LT model may be extended in order to treat screw dislocations where the kink and antikink are asymmetrical.

ACKNOWLEDGMENTS

We thank R. Gröger and V. Vitek for a very fruitful discussion on the comparison between the approach of Ref. 23 and the one used here.

[1] D. Caillard and J. Martin, *Thermally Activated Mechanisms of Crystal Plasticity* (Pergamon, New York, 2003).
[2] R. Peierls, Proc. Phys. Soc. London **52**, 34 (1940).
[3] V. Vitek, Cryst. Lattice Defects **5**, 1 (1974).
[4] L. Kubin, Rev. Deform. Behav. Mater. **1**, 244 (1977).
[5] A. Seeger, Philos. Mag. **1**, 651 (1956).
[6] J. Friedel, *Dislocations* (Pergamon, London, 1964).
[7] A. Seeger and P. Schiller, in *Physical Acoustics*, edited by W. Mason (Academic, New York, 1966), Vol. IIIA.
[8] A. Seeger, in *Dislocation 1984*, edited by J. C. P. Veyssière and L. Kubin (CNRS, Paris, 1984).
[9] A. Scott, *Nonlinear Science* (Oxford University, New York, 2003).
[10] M. Peyrard and T. Dauxois, *Physics of Solitons* (Cambridge University Press, Cambridge, England, 2006).
[11] M. Büttiker and R. Landauer, Phys. Rev. Lett. **43**, 1453 (1979).
[12] M. Büttiker and R. Landauer, Phys. Rev. A **23**, 1397 (1981).
[13] D. Brunner and J. Diehl, Phys. Status Solidi A **124**, 455 (1991).
[14] A. H. W. Ngan and M. Wen, Phys. Rev. Lett. **87**, 075505 (2001).
[15] D. Rodney, Phys. Rev. B **76**, 144108 (2007).
[16] M. Wen and A. Ngan, Acta Mater. **48**, 4255 (2000).
[17] H. Jónsson, G. Mills, and K. Jacobsen, in *Classical and Quantum Dynamics in Condensed Phase Simulations*, edited by G. Berne and D. Coker (World Scientific, Singapore, 1998), p. 385.
[18] L. Pizzagalli, A. Pedersen, A. Arnaldsson, H. Jónsson, and P. Beauchamp, Phys. Rev. B **77**, 064106 (2008).
[19] J. Chaussidon, M. Fivel, and D. Rodney, Acta Mater. **54**, 3407 (2006).
[20] L. Ventelon and F. Willaime, J. Comput.-Aided Mater. Des. **14**, 85 (2007).
[21] C. Woodward and S. I. Rao, Phys. Rev. Lett. **88**, 216402 (2002).
[22] M. Mrovec, R. Gröger, A. G. Bailey, D. Nguyen-Manh, C. Elsässer, and V. Vitek, Phys. Rev. B **75**, 104119 (2007).
[23] R. Gröger and V. Vitek, Acta Mater. **56**, 5426 (2008).
[24] F. Ercolessi and J. Adams, Europhys. Lett. **26**, 583 (1994).
[25] D. Bacon, Y. Osetsky, and D. Rodney, in *Dislocations in Solids*, edited by J. P. Hirth and L. Kubin (Elsevier North-Holland Publishing Company, Amsterdam, 2008).
[26] M. I. Mendelev, S. Han, D. J. Srolovitz, G. J. Ackland, D. Y. Sun, and M. Asta, Philos. Mag. **83**, 3977 (2003).
[27] C. Domain and G. Monnet, Phys. Rev. Lett. **95**, 215506 (2005).
[28] G. Henkelman and H. Jónsson, J. Chem. Phys. **113**, 9978 (2000).
[29] G. Henkelman, B. Uberuaga, and H. Jónsson, J. Chem. Phys. **113**, 9901 (2000).
[30] H. Suzuki, *Dislocation Dynamics* (McGraw-Hill, New York, 1968).
[31] S. Takeuchi, Philos. Mag. A **39**, 661 (1979).
[32] A. H. W. Ngan, Philos. Mag. Lett. **72**, 11 (1995).
[33] G. de Wit and J. Koehler, Phys. Rev. **116**, 1113 (1959).
[34] J. Hirth and J. Lothe, *Theory of Dislocations* (Wiley, New York, 1982).
[35] L. Yang, P. Soderlind, and J. Moriarty, Philos. Mag. A **81**, 1355 (2001).
[36] L. Ventelon, F. Willaime, and P. Leyronnas, J. Nucl. Mater. (to be published).
[37] W. Press, S. Teukolsky, W. Vetterling, and B. Flannery, *Numerical Recipes* (Cambridge University Press, Cambridge, England, 1996).
[38] D. Rodney and L. Proville, Phys. Rev. B **78**, 104115 (2008).
[39] A. Seeger and U. Holzwarth, Philos. Mag. **86**, 3861 (2006).
[40] J. Dorn and S. Rajnak, Trans. Metall. Soc. AIME **230**, 1052 (1964).
[41] P. Guyot and J. Dorn, Can. J. Phys. **45**, 983 (1967).
[42] A. Couret and D. Caillard, J. Phys. III **1**, 885 (1991).
[43] M. Duesbery and P. Hirsch, in *Dislocation Dynamics*, edited by A. Rosenfield, G. Hahn, A. Bement, and R. Jaffee (McGraw-Hill, New York, 1967).
[44] A. Seeger, Z. Metallkd. **72**, 369 (1981).
[45] B. Joós, Solid State Commun. **42**, 709 (1982).
[46] F. Kroupa and L. Brown, Philos. Mag. **6**, 1267 (1961).
[47] J. Eshelby, Proc. R. Soc. London, Ser. A **266**, 222 (1962).
[48] W. Püschl, G. Schoeck, and H. Kirchner, Philos. Mag. A **56**, 553 (1987).
[49] G. Schoeck, Philos. Mag. **87**, 1631 (2007).
[50] M. Duesbery and Z. Basinski, Acta Metall. Mater. **41**, 643 (1993).